Swing- attenuation for a quadrotor transporting a cable suspended payload

M. Eusebia Guerrero-Sánchez, D. Alberto Mercado-Ravell, Rogelio Lozano, C. Daniel García-Beltrán

Swing-Attenuation for a Quadrotor Transporting a Cable-Suspended Payload

M. E. Guerrero [a,b], D. A. Mercado [a], R. Lozano [a] and C. D. García [b]

[a] *Sorbonne universités, Université de technologie de Compiègne, CNRS, Heudiasyc UMR 7253, CS 60 319, 60 203 Compiègne cedex*

[b] *Centro Nacional de Investigación y Desarrollo Tecnológico, México*

Abstract

This paper presents the problem of safe and fast transportation of packages by an Unmanned Aerial Vehicle (UAV) kind quadrotor. A mathematical model and a control strategy for a special class of underactuated mechanical systems, composed of a quadrotor transporting a cable-suspended payload, is proposed. The Euler-Lagrange formulation is used to obtain the dynamic model of the system, where the integrated dynamics of the quadrotor, cable and payload are considered. An Interconnection and Damping Assignment-Passivity Based Control (IDA-PBC) is chosen because of its inherent robustness. Two cases are considered to obtain two different control laws, in the first case, the designed control law depends on the swing angle of the cable, in the second case the control law does not depend on it. The control objective is to transport the payload from point to point, with swing reduction along trajectory. Experimental results using a monocular vision based navigation are shown to evaluate the proposed control law.

1 Introduction

The autonomous aerial transportation of a cable-suspended payload is an interesting and important topic that has attracted the research interest in recent years. It can be applied to a wide range of useful tasks, such as deploying supplies in military operations, or delivering first-aid kits for personal assistance to the victims in disasters like floods, earthquakes, fires, industrial accidents, among others. It is also a basic technology for other future applications, such as, building platforms in hazardous environments [1]. Even more, important global companies for delivery services have announced their wide interest in using UAVs in the short term for package delivery.

These applications often require aggressive maneuvers for fast transportation of fragile payloads. The pendulum like behavior of the slung load gives a high risk of oscillations that can result in dangerous situations [2]. Furthermore, unstable oscillations can occur at high speeds due to the different aerodynamic shapes of the slung loads. Hence, it is very important to cancel or reduce oscillations of the suspended payload to avoid damage on the load, the environment and the people around and guarantee safety in the operation.

In such context, one can choose between several approaches. For example, one option is to design control strategies that stabilize the oscillation to zero [3]-[10]. Another approach is applying control techniques to solve swing-free trajectory tracking [11]-[22].

The design of controllers that rapidly stabilize the payload swing and the general problem of an UAV transporting a cable-suspended payload, as the one depicted in Figure 1, has been investigated in a few recent works. For example, [3] presents an adaptative controller for a quadrotor transporting a point-mass payload connected by a flexible

⋆ This work was supported by CONACYT.

Email addresses: maria-eusebia.guerrero-sanchez@hds.utc.fr (M. E. Guerrero), dmercado@hds.utc.fr (D. A. Mercado), rlozano@hds.utc.fr (R. Lozano), cgarcia@cenidet.edu.mx (C. D. García).

Fig. 1. Experimental platform for a quadrotor with a cable-suspended payload.

cable. The cable is modeled as serially-connected rigid links and the payload is modeled as a point-mass. Meanwhile, [4] explores the effect of dynamic load disturbances introduced by instantaneously increased payload mass and how this affect a quadrotor under proportional integral derivative flight control. [5] proposes a nested saturation controller to stabilize the system and to control the oscillations of the suspended load. The control law guarantees asymptotic stability without any restrictions on the position and velocity of the aerial vehicle. [6] introduces a nonlinear controller to stabilize the quadrotor and the load, during positioning and trajectory tracking tasks. Also, experiments of transportation and accurate deployment of payloads with single/multiple autonomous aerial vehicles are presented in [7]. Moreover, [8] develops a geometric nonlinear control to exponentially stabilize the position of the quadrotor while aligning the links to the vertical direction below the quadrotor. As well, a geometric control but for multiple quadrotors transporting a rigid-body load is also developing in [9]. A model based algorithm controller in order to control the position and attitude of the system of interest is used in [10].

On the other hand, for the swing-free trajectory tracking, a technique based on dynamic programming is proposed in [11]. In addition, [12] presents an adaptive controller considering changes in the center of gravity and an optimal trajectory generation also based on dynamic programming. [13] introduces a model-free approach for solving this problem involving a reinforcement learning algorithm. Similarly, [14] and [15] integrates the swing-free path tracking and sampling-based path planning to solve the aerial cargo delivery task. In that work, each of the modules is evaluated separately, and showed that learning converges to a single policy, and performs minimal residual oscillation delivery task. Also, [16] proposes a method for learning control of nonlinear motion systems through combined learning of state-value and action-value functions applied to an UAV carrying a suspended load. [17] and [18] present an online control policy based on supervised machine learning, Least Squares Axial Sum Policy Approximation (LSAPA), that generates trajectories for robotic preference-balancing tasks under stochastic disturbances. [19] and [20] extend this issue by defining an hybrid system for the lift maneuver for the case of a planar version of the problem. They demonstrate that the hybrid model is indeed a differentially-flat hybrid system. Moreover, [21] and [22] use the differentially-flat property to design trajectories and preliminary results have been demonstrated in simulations and in experiments for a quadrotor transporting a cable-suspended load along the longitudinal plane.

However, in the above mentioned works, the control laws explicitly depend on the swing angle of the cable, and therefore, they require extra sensors to measure it or designing an observer to estimate it. Furthermore, experimental results are usually obtained with the help of an expensive motion capture system. In this article the IDA-PBC methodology is used for precise and fast payload positioning with asymptotic stabilization of the swing angle to the minimum of the desired energy function in a short time, without dependance on the angle of oscillation (second case), and without requiring an external motion capture system for the implementation.

There are some works where IDA-PBC is applied to UAVs. For example, [23] develops a robust control of under-actuated aerial manipulators via IDA-PBC, while, [24] presents a nonlinear control technique based on passivity to solve the path tracking problem for the quadrotor. As well, a controller for a VTOL aircraft via PBC methodology is designed in [25]. There, the path tracking problem is solved for a realistic quadrotor model, in addition, an integral control action is added to the control strategy for sustained disturbance rejection. Also, [26] proposes a damping assignment passivity-based controller that is able to change the apparent dynamical parameters of a quadrotor.

In our previous work [27], we studied the problem of a quadrotor with a cable-suspended payload but only within the longitudinal plane. The two-dimensional mathematical model was obtained and a simple PBC strategy, without total

energy-shaping, is designed. It only presented numerical simulations to validate the control approach. Then, in [28] the dynamical model was extended to the three-dimensional case and real-time experimental results were included. In the present work, the mathematical model is obtained via the Euler-Lagrange formalism for a quadrotor transporting a cable-suspended payload evolving in a three-dimensional space. The novelty with respect to our previous works is that the mathematical model is represented in two different ways, according to the control objectives. In the first model, the inertia matrix $\mathcal{M}$ depends on the angle of oscillation. In the second model, the inertia matrix $\mathcal{M}$ does not depend on this angle and this simplifies the energy-shaping phase of the IDA-PBC strategy. Moreover, the IDA-PBC methodology is used to incorporate information about the underactuated system structure and to deal with the concept of energy in the control strategy. Then, two cases are considered to obtain two different control laws for planar maneuvers and compare the obtained performances. In contrast to [27] and [28], the kinetic energy-shaping is included for both controllers. In the first case, the designed control law depends on the swing angle of the cable, but the total energy is shaped. On the other hand, the second control law does not explicitly depend on the swing angle, hence, no extra measurement is required. However, the energy-shaping only acts on the actuated coordinates.

In short, the main contribution of this paper is to present a nonlinear dynamic model and two control systems, for a quadrotor UAV with a cable-suspended payload that explicitly incorporate a total energy-shaping. Also, real-time experimental results are presented using monocular vision based navigation, demonstrating the validity and good performance of the control scheme. Real-time validation of similar algorithms can be found in the literature, nevertheless they usually use expensive motion capture systems, as VICON and OptiTrack systems. In our work, we validate the proposed algorithm using an inexpensive localization system based only in a monocular camera fused with inertial sensors. This localization system can be adapted and used quickly in several environments. This is also a practical contribution in our work, and in our best knowledge this localization system has not been used before for experiences with quadrotors transporting a payload. An External motion capture system was used only to obtain the graph of the payloads swing angles of the experimental results presented in the paper.

This article is organized as follows: the mathematical model of a three-dimensional quadrotor transporting a cable-suspended payload is described in section II. The control strategy: Interconnection and Damping Assignment-Passivity Based Control is developed in section III. Experimental results are presented in section IV. Conclusions and perspectives are finally given in section V.

2 DYNAMIC MODEL

In this section, a brief description of the model is presented. Figure 2 shows a quadrotor with a payload connected by a cable. The system under consideration has eight degrees of freedom and only four degrees are actuated.

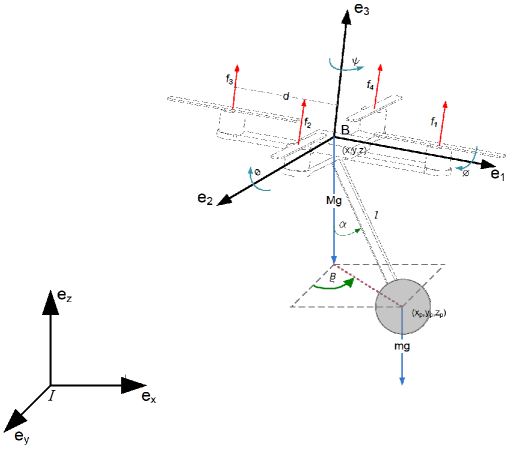

Fig. 2. Three-dimensional quadrotor with a cable-suspended payload.

To facilitate the control design, the dynamic model for a quadrotor with a swinging load, is based on the following assumptions:

(1) The cable connecting payload and helicopter fuselage is rigid, massless and inelastic.

(2) The length of the connecting cable is constant and known.
(3) The angle of the payload is restricted according to the following inequality $-\pi/2 < \alpha < \pi/2$.
(4) The payload can be considered as a mass point.
(5) The aerodynamic effects on the load are neglected.

According to Figure 2, the following notation is used, let us consider an inertial coordinate frame $I = \{e_x, e_y, e_z\}$, fixed to the ground and a body fixed coordinate frame $B = \{e_1, e_2, e_3\}$ which coincides with the center of mass of the quadrotor. Then, the configuration variables are $q = \begin{bmatrix} \xi & \eta & \mu \end{bmatrix}^T \in \Re^8$, where $\xi \triangleq \begin{bmatrix} x & y & z \end{bmatrix}^T \in \Re^3$ denotes the position of the center of mass of the UAV relative to the fixed inertial frame O, $\eta \triangleq \begin{bmatrix} \psi & \theta & \phi \end{bmatrix}^T \in \Re^3$ are the Euler angles yaw, pitch and roll, respectively. $\mu \triangleq \begin{bmatrix} \alpha & \beta \end{bmatrix}^T \in \Re^2$ denotes the swing angles of the cable. l is the length of the cable, while d is the distance between the motors. Finally, f_1, f_2, f_3 and f_4 are the thrust forces provided by each rotor.

The control input is defined as $u = \begin{bmatrix} f & \tau \end{bmatrix}^T \in \Re^4$, where $f = f_1 + f_2 + f_3 + f_4$ is the total thrust magnitude, $\tau = \begin{bmatrix} \tau_\psi & \tau_\theta & \tau_\phi \end{bmatrix}^T$, $\tau_\psi = \Sigma_{i=1}^4 \tau_{M_i}$, $\tau_\theta = (f_2 - f_4)d$ and $\tau_\phi = (f_3 - f_1)d$ are the input torques, as τ_{M_i} is the moment produced by motor M_i, $i = 1, ..., 4$, around the center of gravity of the aircraft. R is the rotational matrix from the body frame to the inertial one, which using the short notation $s_\theta = \sin(\theta)$, $c_\theta = \cos(\theta)$ and $t_\theta = \tan(\theta)$ is given by

$$R = \begin{bmatrix} c_\psi c_\theta & -s_\psi c_\phi + c_\psi s_\theta s_\phi & s_\psi s_\phi + c_\psi s_\theta c_\phi \\ s_\psi c_\theta & c_\psi c_\phi + s_\psi s_\theta s_\phi & -c_\psi s_\phi + s_\psi s_\theta c_\phi \\ -s_\theta & c_\theta s_\phi & c_\theta c_\phi \end{bmatrix}$$

2.1 Euler-Lagrange equations

Under these assumptions, the mathematical model is obtained via the Euler-Lagrange formalism. The expressions for the kinetic and potential energy will be presented in order to obtain the Lagrangian of the system. The total kinetic energy function $K(q, \dot{q})$ of the quadrotor transporting a cable-suspended payload, resulting from the translational and rotational motion can be partitioned as the sum of the quadrotor kinetic energy

$$K_{UAV} = \frac{1}{2} M \dot{\xi}^T \dot{\xi} + \frac{1}{2} \dot{\eta}^T J \dot{\eta} \tag{1}$$

and the cable-suspended payload kinetic energy

$$K_p = \frac{1}{2} m \dot{\xi}_p^T \dot{\xi}_p + \frac{1}{2} I_p (\dot{\alpha}^2 + \dot{\beta}^2) \tag{2}$$

where the matrix $J = J(\eta)$ acts as the inertia matrix for the full rotational kinetic energy of the quadrotor expressed in terms of the generalized coordinates η (for further details, the interested reader is referred to [29]), and is defined as

$$J = \begin{bmatrix} I_\psi s_\theta^2 + I_\theta c_\theta^2 s_\phi^2 + I_\phi c_\theta^2 c_\phi^2 & c_\theta c_\phi s_\phi (I_\theta - I_\phi) & -I_\psi s_\theta \\ c_\theta c_\phi s_\phi (I_\theta - I_\phi) & I_\theta c_\phi^2 + I_\phi s_\phi^2 & 0 \\ -I_\psi s_\theta & 0 & I_\psi \end{bmatrix}$$

In the above expressions, I_p is the mass moment of inertia of the payload, I_ψ, I_θ and I_ϕ are the mass moments of inertia of the quadrotor, while M and m represent the mass of the quadrotor and the payload, respectively. Finally, the position of the payload center in the cartesian coordinate are denoted by

$$\xi_p = \xi + l\mathbf{r}, \tag{3}$$

with $\xi_p = \begin{bmatrix} x_p & y_p & z_p \end{bmatrix}^T$ and $\mathbf{r} = \begin{bmatrix} s_\alpha c_\beta & s_\alpha s_\beta & -c_\alpha \end{bmatrix}^T$. Then, The total kinetic energy function $K(q, \dot{q})$ is

$$K(q,\dot{q}) = \frac{1}{2}M\dot{\xi}^T\dot{\xi} + \frac{1}{2}\dot{\eta}^T J\dot{\eta} + \frac{1}{2}m\dot{\xi}_p^T\dot{\xi}_p + \frac{1}{2}I_p(\dot{\alpha}^2 + \dot{\beta}^2) \tag{4}$$

The total potential energy function $V(q)$ of the system results from the sum of the potential energy of the quadrotor and the cable-suspended payload as

$$V(q) = Mgz + mg(z - lc_\alpha) \tag{5}$$

Using (4) and (5), the lagrangian may be written as

$$\begin{aligned} L = &\frac{1}{2}(M+m)(\dot{x}^2 + \dot{y}^2 + \dot{z}^2) + \frac{1}{2}(I_\psi s_\theta^2 + I_\theta c_\theta^2 s_\phi^2 + I_\phi c_\theta^2 c_\phi^2)\dot{\psi}^2 + \frac{1}{2}(I_\theta c_\phi^2 + I_\phi s_\phi^2)\dot{\theta}^2 - I_\psi s_\theta \dot{\psi}^2\dot{\phi}^2 \\ &+(I_\theta c_\theta c_\phi s_\phi - I_\phi c_\theta c_\phi s_\phi)\dot{\psi}^2\dot{\theta}^2 + \frac{1}{2}I_\psi\dot{\phi}^2 + ml\dot{\beta}s_\alpha(c_\beta\dot{y} - s_\beta\dot{x}) + ml\dot{\alpha}c_\alpha(s_\beta\dot{y} + c_\beta\dot{x}) + \frac{1}{2}ml^2\dot{\alpha}^2 \\ &+\frac{1}{2}ml^2 s_\alpha^2\dot{\beta}^2 + ml\dot{z}s_\alpha\dot{\alpha} + \frac{1}{2}I_p(\dot{\alpha}^2 + \dot{\beta}^2) - Mgz - mg(z - lc_\alpha) \end{aligned} \tag{6}$$

By applying the Euler-Lagrange formulation,

$$\frac{d}{dt}\left(\frac{\partial L}{\partial \dot{q}}\right) - \frac{\partial L}{\partial q} = bu \tag{7}$$

we obtain the equations modeling the total motion of the system expressed in matrix form as

$$\mathcal{M}(q)\ddot{q} + C(q,\dot{q})\dot{q} + G(q) = bu \tag{8}$$

where $\mathcal{M}(q) \in \Re^{8\times 8}$ is the inertia matrix, which is symmetric and positive definite, $C(q,\dot{q}) \in \Re^{8\times 8}$ is the Coriolis and centrifugal matrix, $G(q) \in \Re^8$ is the gravitational vector and the matrix $b \in \Re^{8\times 4}$ is determined by the manner in which the control $u \in \Re^4$ is the input of the system, and is not invertible because the system is underactuated. These matrices are given by:

$$\mathcal{M}(q) = \begin{bmatrix} M+m & 0 & 0 & 0 & 0 & 0 & mlc_\alpha c_\beta & -mls_\alpha s_\beta \\ 0 & M+m & 0 & 0 & 0 & 0 & mlc_\alpha s_\beta & mls_\alpha c_\beta \\ 0 & 0 & M+m & 0 & 0 & 0 & mls_\alpha & 0 \\ 0 & 0 & 0 & I_\psi s_\theta^2 + c_\theta^2(I_\theta s_\phi^2 + I_\phi c_\phi^2) & m_{45} & -I_\psi s_\theta & 0 & 0 \\ 0 & 0 & 0 & (I_\theta - I_\phi)(c_\theta s_\phi c_\phi) & m_{55} & 0 & 0 & 0 \\ 0 & 0 & 0 & -I_\psi s_\theta & 0 & I_\psi & 0 & 0 \\ mlc_\alpha c_\beta & mlc_\alpha s_\beta & mls_\alpha & 0 & 0 & 0 & ml^2 + I_p & 0 \\ -mls_\alpha s_\beta & mls_\alpha c_\beta & 0 & 0 & 0 & 0 & 0 & ml^2 s_\alpha^2 + I_p \end{bmatrix}$$

where $m_{45} = (I_\theta - I_\phi)(c_\theta s_\phi c_\phi)$ and $m_{55} = I_\theta c_\phi^2 + I_\phi s_\phi^2$.

$$C(q) = \begin{bmatrix} 0\ 0\ 0 & 0 & 0 & 0 & -ml(c_\alpha s_\beta \dot{\beta} + c_\beta s_\alpha \dot{\alpha}) & -ml(c_\alpha s_\beta \dot{\alpha} + c_\beta s_\alpha \dot{\beta}) \\ 0\ 0\ 0 & 0 & 0 & 0 & ml(c_\alpha c_\beta \dot{\beta} - s_\alpha s_\beta \dot{\alpha}) & ml(c_\alpha c_\beta \dot{\alpha} - s_\alpha s_\beta \dot{\beta}) \\ 0\ 0\ 0 & 0 & 0 & 0 & mlc_\alpha \dot{\alpha} & 0 \\ 0\ 0\ 0 & c_{44} & c_{45} & c_{46} & 0 & 0 \\ 0\ 0\ 0 & c_{54} & c_{55} & c_{56} & 0 & 0 \\ 0\ 0\ 0 & c_{64} & c_{65} & 0 & 0 & 0 \\ 0\ 0\ 0 & 0 & 0 & 0 & 0 & -ml^2 s_\alpha c_\alpha \dot{\beta} \\ 0\ 0\ 0 & 0 & 0 & 0 & ml^2 s_\alpha c_\alpha \dot{\beta} & ml^2 s_\alpha c_\alpha \dot{\alpha} \end{bmatrix}$$

where $c_{44} = I_\psi \dot{\theta} s_\theta c_\theta - (I_\theta + I_\phi)(\dot{\theta} s_\theta c_\theta s_\phi^2) + (I_\theta - I_\phi)\dot{\phi} c_\theta^2 s_\phi c_\phi$, $c_{45} = I_\psi \dot{\psi} s_\theta c_\theta - (I_\theta - I_\phi)(\dot{\theta} s_\theta c_\phi s_\phi + \dot{\phi} c_\theta s_\phi^2) - (I_\theta + I_\phi)(\dot{\psi} s_\theta c_\theta c_\phi^2 - \dot{\phi} c_\theta c_\phi^2)$, $c_{46} = -(I_\psi \dot{\theta} c_\theta - (I_\theta - I_\phi)(\dot{\psi} c_\theta^2 s_\phi c_\phi))$, $c_{54} = \dot{\psi} s_\theta c_\theta(-I_\psi + I_\theta s_\phi^2 + I_\phi c_\phi^2)$, $c_{55} = -(I_\theta - I_\phi)(\dot{\phi} s_\phi c_\phi)$, $c_{56} = I_\psi \dot{\psi} c_\theta + (I_\theta - I_\phi)(-\dot{\theta} s_\theta c_\phi + \dot{\psi} c_\theta c_\phi^2 - \dot{\psi} c_\theta s_\phi^2)$, $c_{64} = -(I_\theta - I_\phi)(\dot{\psi} c_\theta^2 s_\phi c_\phi)$ and $c_{65} = -I_\psi \dot{\psi} c_\theta + (I_\theta - I_\phi)(\dot{\theta} s_\phi c_\phi + \dot{\psi} c_\theta s_\phi^2 - \dot{\psi} c_\theta c_\phi^2)$.

$$G(q) = \begin{bmatrix} 0\ 0\ (M+m)g\ 0\ 0\ 0\ mlgs_\alpha\ 0 \end{bmatrix}^T$$

$$b(q) = \begin{bmatrix} s_\phi s_\psi + c_\phi c_\psi s_\theta & c_\phi s_\theta s_\psi - c_\psi s_\phi & c_\theta c_\phi & 0\ 0\ 0\ 0\ 0 \\ 0 & 0 & 0 & 1\ 0\ 0\ 0\ 0 \\ 0 & 0 & 0 & 0\ 1\ 0\ 0\ 0 \\ 0 & 0 & 0 & 0\ 0\ 1\ 0\ 0 \end{bmatrix}^T$$

This mathematical model can be expressed as

$$(M+m)\ddot{\xi} + ml\ddot{\mathbf{r}} + (M+m)ge_3 = fRe_3 \tag{9}$$

$$J\ddot{\eta} + C_r(\eta, \dot{\eta})\dot{\eta} = \tau \tag{10}$$

$$\mathbf{r} \times (Mgle_3 - flRe_3 + Ml\ddot{\xi}) = 0 \tag{11}$$

In order to simplify the design of the control strategy (specifically the energy-shaping stage), the mathematical model (9) through (11) is expressed so that the inertia matrix does not depend on q, with details in *Appendix A*, the model (8) can also be represented as

$$(M+m)\left(\ddot{\xi}_p + ge_3\right) = (\mathbf{r} \cdot fRe_3 - Ml(\dot{\mathbf{r}} \cdot \dot{\mathbf{r}}))\,\mathbf{r} \tag{12}$$

$$J\ddot{\eta} + C_r(\eta, \dot{\eta})\dot{\eta} = \tau \tag{13}$$

$$Ml\dot{w} = -fR\mathbf{r} \times e_3 \tag{14}$$

where $C_r(\eta, \dot{\eta}) = \begin{bmatrix} c_{44} & c_{45} & c_{46} \\ c_{54} & c_{55} & c_{56} \\ c_{64} & c_{65} & c_{66} \end{bmatrix}$ and $w \in \Re^2$ is the angular velocity of the suspended load. The expressions (12) through (14) are the load position, the quadrotor attitude and the load attitude dynamics, respectively.

Finally, with the objective to represent the behavior of the payload oscillation in a clearer manner, we define the new swing angles α_x with respect to xz plane and β_y with respect to yz plane, as follows

$$\alpha_x = \sin^{-1}(\sin\alpha\cos\beta)$$
$$\beta_y = \tan^{-1}(\tan\alpha\sin\beta)$$

2.2 Simplified dynamic model for the longitudinal plane

With the objective of simplifying the control design, let us consider the system within the longitudinal plane and then in the transverse plane.

Consider the system (12) through (14) within the longitudinal plane (i.e., $y = \beta = \psi = \phi = 0$). Then, the equations for the translational motion are

$$-fc_{(\theta+\alpha)}s_\alpha = (M+m)\ddot{x}_p + Ml\dot{\alpha}^2 s_\alpha \tag{15}$$

$$fc_{(\theta+\alpha)}c_\alpha = (M+m)\left(\ddot{z}_p + g\right) - Ml\dot{\alpha}^2 c_\alpha \tag{16}$$

and the rotational motion

$$\tau_\theta = I_\theta\ddot{\theta} \tag{17}$$

$$-fs_{(\theta+\alpha)} = Ml\ddot{\alpha} \tag{18}$$

This mathematical model can be expressed in the matrix form (8), where the matrices are given by:

$$\mathcal{M} = \begin{bmatrix} M+m & 0 & 0 & 0 \\ 0 & M+m & 0 & 0 \\ 0 & 0 & I_\theta & 0 \\ 0 & 0 & 0 & Ml \end{bmatrix}, \quad C(q,\dot{q}) = \begin{bmatrix} 0\ 0\ 0 & Mls_\alpha\dot{\alpha} \\ 0\ 0\ 0 & -Mlc_\alpha\dot{\alpha} \\ 0\ 0\ 0 & 0 \\ 0\ 0\ 0 & 0 \end{bmatrix} \tag{19}$$

$$G = \begin{bmatrix} 0 \\ (M+m)g \\ 0 \\ 0 \end{bmatrix}, \quad b(q) = \begin{bmatrix} -c_{(\theta+\alpha)}s_\alpha & 0 \\ c_{(\theta+\alpha)}c_\alpha & 0 \\ 0 & 1 \\ -s_{(\theta+\alpha)} & 0 \end{bmatrix}$$

where $q = \begin{bmatrix} x_p & z_p & \theta & \alpha \end{bmatrix}^T$ and $u = \begin{bmatrix} f & \tau_\theta \end{bmatrix}^T$. For the transverse plane a similar model is obtained with $x = \theta = \psi = 0$ and $\beta = \pi/2$.

Under the same conditions, the model (9) through (11) within the longitudinal plane can be expressed as (8), where the matrices are given by:

$$\mathcal{M}(q) = \begin{bmatrix} M+m & 0 & 0 & mlc_\alpha \\ 0 & M+m & 0 & mls_\alpha \\ 0 & 0 & I_\theta & 0 \\ mlc_\alpha & mls_\alpha & 0 & ml^2 \end{bmatrix}, \quad C(q,\dot{q}) = \begin{bmatrix} 0\ 0\ 0 & -mls_\alpha\dot{\alpha} \\ 0\ 0\ 0 & mlc_\alpha\dot{\alpha} \\ 0\ 0\ 0 & 0 \\ 0\ 0\ 0 & 0 \end{bmatrix} \tag{20}$$

$$G(q) = \begin{bmatrix} 0 \\ (M+m)g \\ 0 \\ mlgs_\alpha \end{bmatrix}, \quad b(q) = \begin{bmatrix} s_\theta & 0 \\ c_\theta & 0 \\ 0 & 1 \\ 0 & 0 \end{bmatrix}$$

3 CONTROL STRATEGY

Interconnection and damping assignment is a passivity based control methodology applied to a special class of underactuated mechanical systems, which is based on systems described by the Port Controlled Hamiltonian (PCH) model. This methodology consists in assigning a new PCH model in closed loop with the interconnection and damping assignment.

In the present work, the IDA-PBC methodology is used to incorporate information about the underactuated system structure and to deal with the concept of energy in the control strategy. The main advantage of the IDA-PBC strategy is its inherent robustness with respect to unmodeled dynamics [31] and parametric uncertainties [32].

3.1 General IDA-PBC theory

The basic philosophy of the IDA-PBC strategy is to assign the closed loop dynamics of a Hamiltonian systems with total energy

$$H(q,p) = \frac{1}{2} p^T \mathcal{M}^{-1}(q) p + V(q) \tag{21}$$

where $q \in \Re^n$, $p \in \Re^n$, are the generalized position and momentum, respectively and $H(q,p)$ is the Hamiltonian. The motion equations can be written as

$$\begin{bmatrix} \dot{q} \\ \dot{p} \end{bmatrix} = \begin{bmatrix} 0 & I_n \\ -I_n & 0 \end{bmatrix} \begin{bmatrix} \nabla_q H \\ \nabla_p H \end{bmatrix} + \begin{bmatrix} 0 \\ b(q) \end{bmatrix} u \tag{22}$$

with $I_n \in \Re^{n \times n}$ as the identity matrix, $\nabla_q H = \partial H / \partial q$ and $\nabla_p H = \partial H / \partial p$.

We propose the following form for the desired energy function:

$$H_d(q,p) = \frac{1}{2} p^T {\mathcal{M}_d}^{-1}(q) p + V_d(q) \tag{23}$$

where $\mathcal{M}_d = \mathcal{M}_d^T > 0$ and V_d represent the desired closed loop inertia matrix and potential energy function, respectively. We will require that the function V_d has an isolated minimum at q_*, that is

$$q_* = \arg\min V_d(q) \tag{24}$$

In PBC, the control input is naturally decomposed into two terms,

$$u = u_{es}(q,p) + u_{di}(q,p) \tag{25}$$

where the first term is designed to achieve the energy-shaping and the second one injects the damping. The desired port controlled Hamiltonian dynamics are taken as the following form [30]

$$\begin{bmatrix} \dot{q} \\ \dot{p} \end{bmatrix} = [J_d(q,p) - R_d(q,p)] \begin{bmatrix} \nabla_q H_d \\ \nabla_p H_d \end{bmatrix} \tag{26}$$

where

$$J_d = -J_d^T = \begin{bmatrix} 0 & \mathcal{M}^{-1}\mathcal{M}_d \\ -\mathcal{M}_d\mathcal{M}^{-1} & J_2(q,p) \end{bmatrix}, \quad R_d = R_d^T = \begin{bmatrix} 0 & 0 \\ 0 & bK_v b^T \end{bmatrix} \geq 0$$

with J_2 as a skew-symmetric matrix and $K_v = K_v^T > 0$, both containing design parameters.

The damping injection is achieved through the negative feedback of the new passive output $y = b^T \nabla_p H_d$. Thus, the damping injection term is given by

$$u_{di}(q,p) = -K_v b^T \nabla_p H_d \tag{27}$$

To obtain the energy-shaping term u_{es} of the controller, we replace (25) and (27) in (22) and make it equal to (26) to obtain

$$\begin{bmatrix} 0 & I_n \\ -I_n & 0 \end{bmatrix} \begin{bmatrix} \nabla_q H \\ \nabla_p H \end{bmatrix} + \begin{bmatrix} 0 \\ b(q) \end{bmatrix} u_{es} = \begin{bmatrix} 0 & \mathcal{M}^{-1}\mathcal{M}_d \\ -\mathcal{M}_d\mathcal{M}^{-1} & J_2(q,p) \end{bmatrix} \begin{bmatrix} \nabla_q H_d \\ \nabla_p H_d \end{bmatrix} \tag{28}$$

The first row of the equations is clearly satisfied. The second can be expressed as

$$b u_{es} = \nabla_q H - \mathcal{M}_d\mathcal{M}^{-1}\nabla_q H_d + J_2\mathcal{M}_d^{-1} p$$

In the underactuated case, whereas the $b^\perp(q) \in \Re^{(n-m)\times n}$ is the full rank left annihilator of b, i.e., $b^\perp b = 0$

$$b^\perp\{\nabla_q H - \mathcal{M}_d\mathcal{M}^{-1}\nabla_q H_d + J_2\mathcal{M}_d^{-1} p\} = 0 \tag{29}$$

The energy-shaping term is given by

$$u_{es} = \left(b^T b\right)^{-1} b^T \left(\nabla_q H - \mathcal{M}_d\mathcal{M}^{-1}\nabla_q H_d \; + J_2\mathcal{M}_d^{-1} p\right) \tag{30}$$

Using (23) the PDEs (29) can be separated into terms that depend on p and terms which are independent of p

$$b^\perp \left\{\nabla_q (p^T\mathcal{M}^{-1}p) - \mathcal{M}_d\mathcal{M}^{-1}\nabla_q (p^T\mathcal{M}_d^{-1}p) \; + 2J_2\mathcal{M}_d^{-1} p\right\} = 0 \tag{31}$$

$$b^\perp \left\{\nabla_q V - \mathcal{M}_d\mathcal{M}^{-1}\nabla_q V_d\right\} = 0 \tag{32}$$

3.2 IDA-PBC methodology for a quadrotor transporting a cable-suspended payload

To simplify the control design, let us consider only planar maneuvers. Then, the control problem is to move, in a short time, the payload from any initial position $q_i = \begin{bmatrix} x_i & z_i & \theta_i & \alpha_i \end{bmatrix}^T$, to a final desired position $q_D = \begin{bmatrix} x_D & z_D & \theta_D & \alpha_D \end{bmatrix}^T$, in this case $\theta_D = \alpha_D = 0$. Specifically we apply the IDA-PBC approach to the two models represented by (8) with matrices given by (19) and (20) to achieve a precise positioning of the payload and a swing-attenuation of the cable-suspended payload.

In order to compare them, two different control laws are considered. In the first case, a control scheme with total energy-shaping is designed, however, the control law depends on the oscillation angle. In the second case, the control strategy does not depend on the oscillation angle.

3.2.1 Case 1

In this case the IDA-PBC control strategy is applied to the simplified dynamic model for the longitudinal plane described by (8) and (19). Then, the same technique is employed for the transverse plane.

In the energy-shaping we note that the inertia matrix $\mathcal{M}$ is independent of q and it is constant, hence, we can take $J_2 = 0$ and select $\mathcal{M}_d$ to be a constant matrix [31] of the form.

$$\mathcal{M}_d = \begin{bmatrix} a_1 & 0 & a_2 & a_3 \\ 0 & a_4 & 0 & 0 \\ a_2 & 0 & a_5 & 0 \\ a_3 & 0 & 0 & a_6 \end{bmatrix}, \quad a_1 a_5 a_6 > {a_2}^2 a_6 + {a_3}^2 a_5 \tag{33}$$

where $a_1 = a_4 = 0.4$, $a_2 = a_3 = a_6 = 0.1$ and $a_5 = 0.177$. We have that b is a function of two coordinates, an actuated coordinate θ and another unactuated α, thus the range of $b^\perp$ under these conditions is 1. With $b^\perp = \begin{bmatrix} c_\alpha & s_\alpha & 0 & 0 \end{bmatrix}$, the potential energy PDE (32) takes the form:

$$c_\alpha \left[\frac{a_1}{M+m} \frac{\partial V_d}{\partial x} + \frac{a_2}{I_\theta} \frac{\partial V_d}{\partial \theta} + \frac{a_3}{Ml} \frac{\partial V_d}{\partial \alpha} \right] + s_\alpha \left[\frac{a_4}{M+m} \frac{\partial V_d}{\partial z} - g(M+m) \right] = 0 \tag{34}$$

which is solved and thus the desired energy potential is obtained:

$$V_d = -\frac{g(M+m)Ml}{a_3} \ln(c_\alpha) + \Phi$$

where $\Phi(x, z, \theta, \alpha)$ is an arbitrary differentiable function. Note that the selection of $\Phi(x, z, \theta, \alpha)$ is governed by the condition given by (24). For this, the necessary condition $\nabla_q V_d(q_*) = 0$ and the sufficient condition $\nabla_q^2 V_d(q_*) > 0$ will hold if the Hessian of $\Phi(x, z, \theta, \alpha)$ at q_* is positive [30]. In our case, we choose $\Phi(x, z, \theta, \alpha)$ to be a quadratic function which leads to

$$\begin{aligned} V_d = -\tfrac{g(M+m)Ml}{a_3} \ln(c_\alpha) + \tfrac{1}{2} k_{px} \left(\theta - \tfrac{a_2(M+m)}{a_1 I_\theta}(x - x_D) \right)^2 + \tfrac{1}{2} k_{pz} \left(z - z_D + \tfrac{a_4 Ml}{a_3(M+m)} \ln(c_\alpha) \right)^2 \\ + \quad \tfrac{1}{2} k_{p\alpha} \left(\alpha - \tfrac{a_3 I_\theta}{a_2 Ml} \theta \right)^2 \end{aligned} \tag{35}$$

where $(x_D, z_D, 0, 0)$ denotes the equilibrium configuration and the k_{px}, k_{pz} and $k_{p\alpha}$ terms are proportional gains and are used as tuning parameters. To compute the final control law we first determine the energy-shaping term u_{es} from (30), which, in this case, takes the form:

$$u_{esx} = \begin{bmatrix} s_{(\alpha+\theta)} \left[a_6 \left(\frac{k_{p\alpha}\gamma + (M+m)g\vartheta + \vartheta k_{pz}\delta}{Ml} - \rho a_3 k_{px} \chi \right) \right] + c_{(\alpha+\theta)} c_\alpha \left[g(M+m) - \frac{a_4}{M+m} k_{pz} \delta \right] \\ + c_{(\alpha+\theta)} s_\alpha \left[a_2 \left(I_\theta k_{px} \chi - \varsigma k_{p\alpha} \gamma \right) + a_3 \left(\frac{k_{p\alpha}\gamma + (M+m)g\vartheta + \vartheta k_{pz}\delta}{Ml} \right) - \rho a_1 k_{px} \chi \right] \\ \\ \frac{k_{px}}{I_\theta} \left(\frac{a_2^2 - a_5(M+m)}{(M+m)} \right) \chi + a_5 \varsigma k_{p\alpha} \gamma \end{bmatrix} \tag{36}$$

where

$$\chi(x, \theta) = \theta - \frac{a_2}{I_\theta}(x - x_D), \quad \delta(z, \theta) = z - z_D - \frac{Ml}{a_3} \ln(c_\alpha), \quad \gamma(\alpha, \theta) = \alpha - \frac{I_\theta a_3}{a_2 Ml} \theta, \quad \vartheta(\alpha) = \frac{Ml}{a_3} t_\alpha,$$

$$\rho = \frac{a_2}{I_p(M+m)}, \quad \varsigma = \frac{a_3}{Mla_2}$$

and second we determine the damping injection term u_{di} from (27)

$$u_{dix} = \begin{bmatrix} \lambda a_5(M+m)\dot{x} + \left(\frac{-a_2^2a_6+a_3^2a_5-a_1a_5a_6}{a_4(a_2^2a_6+a_3^2a_5-a_1a_5a_6)}\right)(M+m)c_{(\alpha+\theta)}c_\alpha\dot{z} - \lambda a_6 I_\theta\dot{\theta} + \varpi Ml\dot{\alpha} \\ -\frac{a_2a_6(M+m)}{a_2^2a_6+a_3^2a_5-a_1a_5a_6}\dot{x} - \frac{(a_3^2-a_1a_6)I_\theta}{a_2^2a_6+a_3^2a_5-a_1a_5a_6}\dot{\theta} - \frac{a_2a_3Ml}{a_2^2a_6+a_3^2a_5-a_1a_5a_6}\dot{\alpha} \end{bmatrix} \tag{37}$$

where

$$\lambda = \frac{a_3s_{(\alpha+\theta)} - a_6c_{(\alpha+\theta)}s_\alpha}{a_2^2a_6 + a_3^2a_5 - a_1a_5a_6}, \quad \varpi = \frac{s_{(\alpha+\theta)}(a_2^2 - a_1a_5) + a_3a_5c_{(\alpha+\theta)}s_\alpha}{a_2^2a_6 + a_3^2a_5 - a_1a_5a_6}$$

Stability

Proposition 2: The control law (25) with (36) and (37) guarantees asymptotic stability at the equilibrium of $(q,p) = (q_*, 0) = (x_D, z_D, 0,\ 0, 0, 0, 0, 0)$ with the desired energy function given by (23) with (33) and (35) for any constants satisfying $0 < a_2 < \sqrt{a_1a_5 - \frac{a_3^2a_5}{a_6}}$ and the attraction domain $(q,p) \in \Re^2 \times (-\pi/2, \pi/2) \times (-\pi/2, \pi/2) \times \Re^4$.

Proof. M_d is positive definite for any constants satisfying $0 < a_2 < \sqrt{a_1a_5 - \frac{a_3^2a_5}{a_6}}$, also the desired potential energy function (35) is positive define for any $q \in \Re^2 \times (-\pi/2, \pi/2) \times (-\pi/2, \pi/2)$, then, the desired total energy function is positive definite and is a Lyapunov function.

Then, differentiating (23) along the trajectories of the system

$$\dot{H}_d = p^T M_d^{-1}\dot{p} + [\nabla_q V_d]^T\dot{q}$$

Taking into account that $\nabla_p H_d = M_d^{-1}p$ and $[\nabla_q H_d]^T = [\nabla_q V_d]^T$, we obtain

$$\dot{H}_d = [\nabla_p H_d]^T\dot{p} + [\nabla_q H_d]^T\dot{q}$$

From (26), $\dot{q} = M^{-1}M_d\nabla_p H_d$ and $\dot{p} = -M_dM^{-1}\nabla_q H_d - bK_vb^T\nabla_p H_d$, it follows that

$$\dot{H}_d = [\nabla_p H_d]^T\left(-M_dM^{-1}\nabla_q H_d - bK_vb^T\nabla_p H_d\right) + [\nabla_q H_d]^T\left(M^{-1}M_d\nabla_p H_d\right)$$

Note that $[\nabla_p H_d]^T\left(-M_dM^{-1}\nabla_q H_d\right) = [\nabla_q H_d]^T\left(M^{-1}M_d\nabla_p H_d\right)$, thus, we obtain the following

$$\dot{H}_d = -[\nabla_p H_d]^T bK_v b^T\nabla_p H_d \leqslant 0$$

Using the LaSalle's invariance principle, all the trajectories of the system converge to the equilibrium points and this implies asymptotic stability.

Let X be the set of all points where $\dot{H}_d = 0$. If $\dot{H}_d = 0$, then, $X = \left\{(q,p)\,|\,\dot{H}_d = 0\right\}$. Therefore H_d is constant. Moreover, $\dot{H}_d = 0$ implies that $\nabla_p H_d \in span\left((b^\perp)^T\right)$. If the equilibrium point is $(q_*, 0) \in X$ and $V_d(q_*) = 0$ then, $\dot{H}_d = [\nabla_q H_d]^T\dot{q} = 0$. Hence, $\dot{q} = \nabla_p H_d = 0$ so $p = 0$ or $\nabla_p H_d = 0$. From the above, it can be concluded that in both cases the states remain at the equilibrium.

Simulations

Similarly we can obtain the controller to the simplified dynamic model for the transverse plane. Then, the control law is applied to the mathematical model given in (8) and (19). It is important to notice that the controllers for both two-dimensional dynamic systems are applied separately, i.e., the controller for the longitudinal dynamic is switched to the controller for the transverse dynamic at the second 15. Figure 3 shows the evolution of the states with desired equilibrium condition as $x_D = 3$, $z_D = 1$, $\theta_D = \alpha_{xD} = 0$ for the case of the longitudinal dynamic and $y_D = 4$, $z_D = 2.5$, $\phi_D = \beta_{xD} = 0$ for the transverse dynamic, where it is observed that the simulation goal for the proposed control scheme is accomplished and the control objective is achieved in less than 8 seconds.

Note that the angles α_x and β_y present a reduced swing ($\alpha_x < 2°$ and $\beta_y < 2°$) in less than 1.5 seconds (see Figure 3(c)). This behavior is that fast thanks to the energy-shaping and the fact that the swing angle α is explicitly considered by the controller given by (36) and (37). Concerning the control inputs, Figure 3(d) presents the evolution of f, τ_α and τ_ϕ.

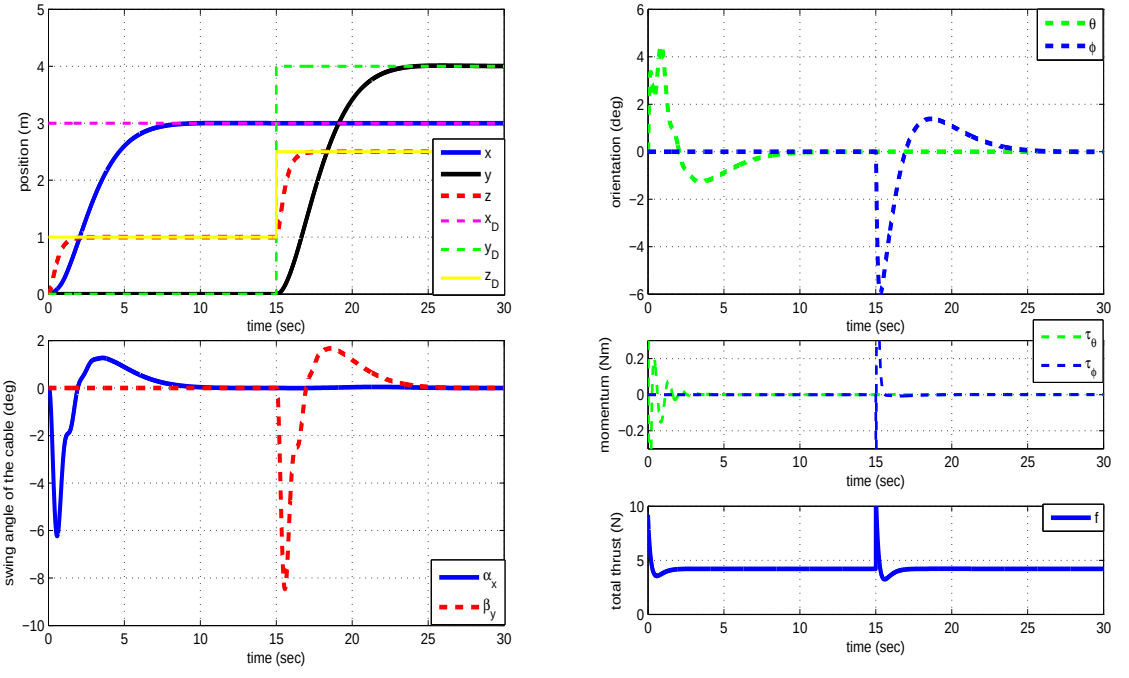

Fig. 3. Simulation results for the states and inputs evolution.

3.2.2 Case 2

Our aim is to find a control law that does not depend on the swing angle. Hence, the mathematical model with a inertia matrix $\mathcal{M}(q)$ described in (8) and (20) is taken into account for the longitudinal plane.

In the energy-shaping phase, we can select $J_2 = 0$, while $\mathcal{M}_d(q)$ is chosen such that the resulting control law will not depend on α, i.e.

$$\mathcal{M}_d(q) = \begin{bmatrix} M+m & 0 & a_{12} & -mlc_\alpha \\ 0 & M+m & 0 & mls_\alpha \\ a_{12} & 0 & I_\theta & 0 \\ -mlc_\alpha & mls_\alpha & 0 & ml^2 \end{bmatrix} > 0$$

note how $\mathcal{M}_d(q)$ is very similar to $\mathcal{M}(q)$ in (20) and the q-dependent terms are exactly the same. Then, the energy-shaping term of the controller (30) is reduced to

$$u_{es} = \left(b^T b\right)^{-1} b^T \left(\nabla_q H - \mathcal{M}_d \mathcal{M}^{-1} \nabla_q H_d\right) \tag{38}$$

Under these conditions and with $b^\perp = \begin{bmatrix} -c_\theta & s_\theta & 0 & 0 \\ 0 & 0 & 0 & 1 \end{bmatrix}$, the potential energy PDE (32) takes the form:

$$\begin{gathered} c_\theta \left[\frac{\partial V_d}{\partial x} + \frac{a_{12}}{I_\theta}\frac{\partial V_d}{\partial \theta}\right] - s_\theta \left[\frac{\partial V_d}{\partial z} - g(M+m)\right] = 0 \\ glms_\alpha - \frac{\partial V_d}{\partial \alpha} = 0 \end{gathered} \tag{39}$$

which is solved and thus the desired energy potential is obtained:

$$V_d = -glm(c_\alpha) + \frac{g(M+m)I_\theta}{a_{12}} \ln(c_\theta) + \Phi$$

Analogously to the former case, $\Phi(x, z, \theta)$ is picked out as a quadratic function

$$V_d = -glm(c_\alpha) + \frac{g(M+m)I_\theta}{a_{12}} \ln(c_\theta) + \frac{1}{2}k_{px}\left(\theta - \frac{a_{12}(x - x_D)}{I_\theta}\right)^2 + \frac{1}{2}k_{pz}\left(z - z_D - \frac{I_\theta}{a_{12}} \ln(c_\theta)\right)^2$$

To compute the final control law for this case, we first determine the energy-shaping term u_{es} from (38), which, in this case, takes the form:

$$u_{esx} = \begin{bmatrix} c_\theta \left(k_{pz}\left(z - z_d + \frac{I_\theta}{a_{12}} \ln(c_\theta)\right) + g(M+m)\right) + \frac{k_{px} a_{12} s_\theta}{I_\theta}\left(\theta - \frac{a_{12}}{I_\theta}(x - x_d)\right) \\ \frac{k_{px}}{I_\theta}\left(\theta - \frac{a_{12}}{I_\theta}(x - x_d)\right) + \frac{I_\theta g(M+m)}{a_{12}} t_\theta + k_{pz}\frac{I_\theta}{a_{12}} t_\theta \left(z - z_d + \frac{I_\theta}{a_{12}} \ln(c_\theta)\right) \end{bmatrix} \tag{40}$$

and second we determine the damping injection term u_{di} from (27)

$$u_{dix} = \begin{bmatrix} k_b\left(\frac{a_{12}}{\kappa}\dot{x} - \frac{(M+m)}{\kappa}\dot{\theta}\right) - k_a s_\theta \left(\frac{I_\theta}{\kappa}\dot{x} - \frac{a_{12}}{\kappa}\dot{\theta}\right) - k_a c_\theta \frac{1}{M+m}\dot{z} \\ k_c\left(\frac{a_{12}}{\kappa}\dot{x} - \frac{(M+m)}{\kappa}\dot{\theta}\right) - k_b s_\theta \left(\frac{I_\theta}{\kappa}\dot{x} - \frac{a_{12}}{\kappa}\dot{\theta}\right) - k_b c_\theta \frac{1}{M+m}\dot{z} \end{bmatrix} \tag{41}$$

where $\kappa = I_\theta(M+m) - a_{12}$ and k_a, k_b, k_c are the K_v matrix terms that act on the derivatives of the error and inject damping into the system.

Simulations

Simulations were carried out to test the performance of the new proposed control law, in a similar way to the previous case. Some results are presented through Figure 4, where the evolution of the states are depicted, with desired equilibrium condition as $x_D = 3$, $z_D = 1$, $\theta_D = \alpha_{xD} = 0$ for the case of the longitudinal dynamic and $y_D = 4$, $z_D = 2.5$, $\phi_D = \beta_{xD} = 0$ for the transverse dynamic. It can be seen that the control objective is achieved in less than 10 seconds, as can be seen from Figure 4(c) where the swing angles remain small ($\alpha_x < 2^\circ$ and $\beta_y < 2^\circ$ after 5 seconds), in spite of not being explicitly considered by the control law (40), (41). This behaviour prevents the use of extra sensors to measure these angles. Concerning the control inputs, Figure 4(d) presents the evolution of f, τ_α and τ_ϕ.

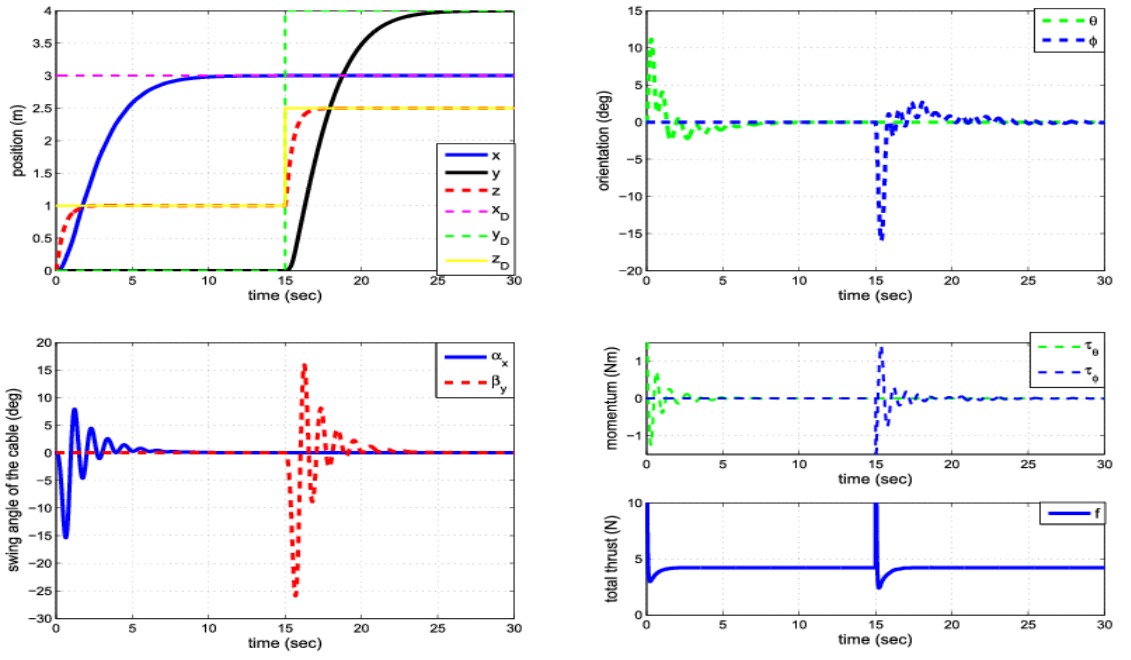

Fig. 4. Simulation results for the states and inputs evolution.

The main difference between the two cases is that, in the first case the control law depends on the swing angle and in the second case, the control law does not depend on it. This is accomplished by choosing a suitable $\mathcal{M}_d$ matrix. However, the choice of the controller depends on the requirements. We can choose between a fast controller that explicitly depends on α (first case) and a controller not so fast that does not depend on it. The main advantage for the practical implementation of the second case is that it does not require an extra measurement for the oscillation angle. However, in the energy-shaping phase the same terms of the matrix $\mathcal{M}$ which depend on not-actuated coordinates, are selected for the matrix $\mathcal{M}_d$.

4 REAL-TIME EXPERIMENTS

4.1 Experimental Setup

In order to validate the proposed control strategy, an experimental platform was developed. It consists of a low-cost commercial quadrotor kind Parrot AR.Drone, with an extra payload attached to it by a two-degrees of freedom rigid rod, as showed in Figure 1. However, in order to avoid interferences with the down-looking sensors, such as the ultrasonic sensor and the camera used for the optic flow calculation, the cable-suspended payload is not centered at the body frame, instead it is placed at the rear. The AR.Drone measures $53 \times 52cm$, weights $0.42kg$ and offers robustness to crashes. Meanwhile, the added payload weights about $0.05kg$ and the cable measures $40cm$. The considered UAV is equipped with three-axis gyroscopes and accelerometers, an ultrasonic altimeter, an air pressure sensor and a magnetic compass. It also provides videos from two cameras. The first one is looking downwards with a resolution of 320×240 pixels at a rate of 60fps, and is used to estimate the horizontal velocities by means of optic flow. The second camera is looking forward and has a resolution of 640×360 at 30fps. This latter is used for monocular vision based navigation. However, neither the software nor the hardware can be modified easily from the AR.Drone. All sensor measurements are sent to a ground station at a frequency of $200Hz$.

A vision-based navigation algorithm that consists of a monocular Simultaneous Localization and Mapping (SLAM) and an Extended Kalman Filter (EKF) data fusion algorithms is employed. The solution for monocular SLAM is based on Parallel Tracking and Mapping (PTAM) [33], where the tracking and mapping are split into two different tasks and are processed in parallel, resulting in a nice method for estimating camera pose in an unknown scene. It was originally conceived for augmented reality applications and then successfully extended for micro aerial vehicles (MAVs) localization [34], [35], and released as open-source software for Robot Operating System (ROS). For more

details see [35], [36]. This navigation algorithm is computed at a ground station computer with ROS, along with the proposed control strategy.

Finally, an OptiTrack motion capture system is used to estimate the swing angles for the payload. It consists of a set of twelve infrared cameras capable of tracking the pose of an object from a set of spheres markers. It is important to note that the described system does not depend on the motion capture system, and it is only used to obtain the graph of the payload's swing angles.

4.2 Experimental Results

The proposed passivity based control strategy for a quadrotor with a cable-suspended payload was successfully implemented and tested, for planar maneuvers in the longitudinal and the transverse planes, one at a time, using the previously described experimental platform. The ψ state is controlled by means of a proportional derivative controller. The practical objective was to transport the payload, fast and with reduced swing, through different given way-points with a separation of $2m$ from each other. Please note that the rigid rod is not centered for the y axis, producing a slight difference in the behavior along each axis. Several tests were carried out and the results can be studied through Figures 5-9. Also, a video can be watched at `https://www.youtube.com/watch?v=XAuI_3_uIUM`.

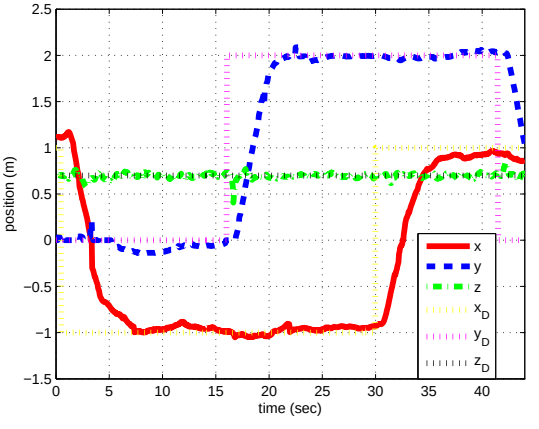

Fig. 5. Quadrotor position.

Figure 5 displays the position of the quadrotor during the test. We can notice that huge changes in position are demanded and accomplished in a short time, about $2m$ in $5s$. Figure 6 presents the payload swing angles α_x and β_y. Remember that the main objective of this works is to stabilize these angles while transporting the payload. We can observe in Figure 6 the good behavior of the overall system since the swing angles always remains well bounded in small values, with a Root Mean Square (RMS) oscillation of 4.3592^o and 5.9379^o for α_x and β_y, respectively, and seldom bigger than 15^o only when there are changes of trajectories in the seconds 0.5, 16, 30 and 41.5. These changes are represented by the black vertical lines in Figure 6. Despite the absence of a direct measurement of the swing angles, the proposed control strategy is able to accomplish satisfactorily its goal.

The quadrotor attitude is presented in Figure 7, while the control inputs are depicted at Figure 8. Finally, a three-dimensional view of the trajectory followed by the UAV during the experiment is shown in Figure 9, where we can observe the consistency and good performance of the control strategy and the experimental setup, in spite of the lack of an expensive motion capture system or any other external reference for positioning.

Several trials were performed and some of the obtained results are presented on the Tables 1 and 2, where we measured in each cycle the RMS, the setting time (T_s), the final swing (FS) and the maximum swing (MS). The different trials were performed for the same regulation problem of transporting the load for $2m$ in each axis, under similar conditions. The observed variation along the different trials can be explained for the delays and uncertainties introduced by the vision system for positioning, as well as some noise in the measurement of the swing angle. The vision navigation system offers a good inexpensive alternative for localization without the need of any special external marker or motion capture system. On the other hand, variations on the results for each coordinate, x and y, is explained due to the fact that the load is not well aligned with respect to the center of mass of the

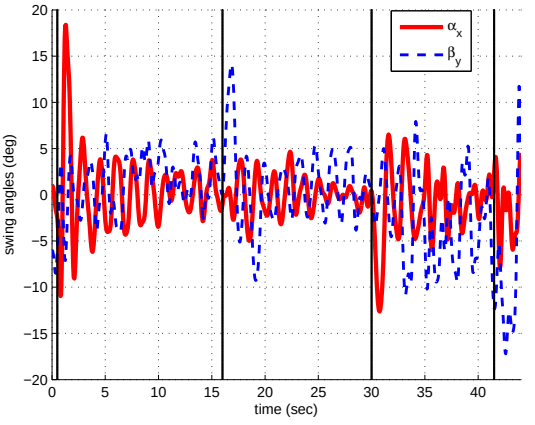

Fig. 6. Swing angles α_x and β_y.

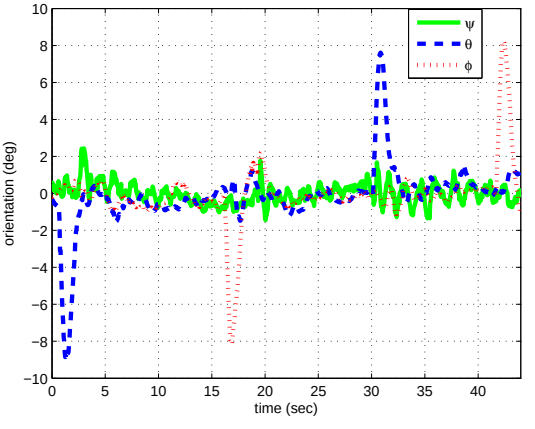

Fig. 7. Quadrotor attitude.

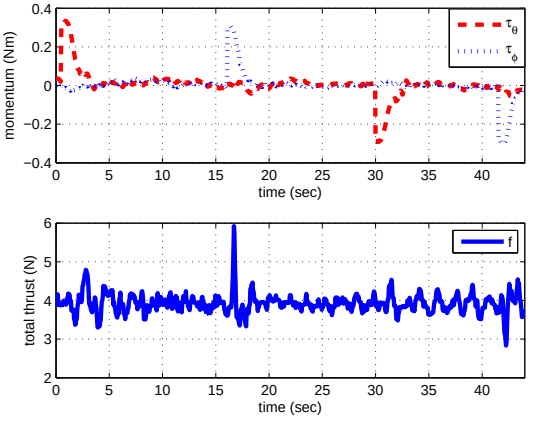

Fig. 8. Control inputs responses.

quadrotor because it caused interference with the down-looking sensors attached at the bottom of the UAV, such as the ultrasound altitude sensor and the camera for measure the optic flow.

The experimental results were compared with some related published results. For example, in [6] T_s =3s, MS= 11^o

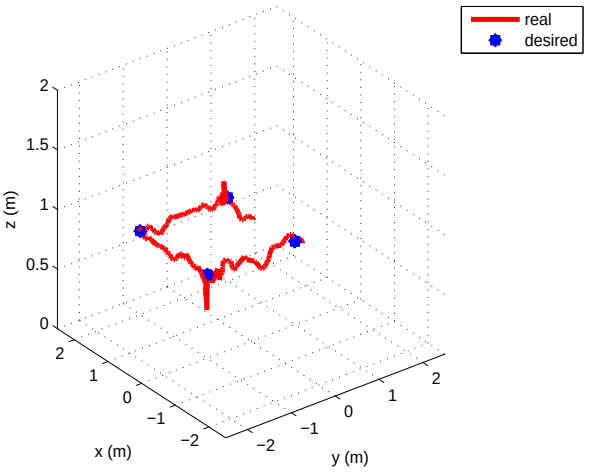

Fig. 9. Three-dimensional trajectory.

and FS=2^o, with $M = 0.5kg$, $m = 0.1kg$ and $l = 50cm$, here the payload is moved $1m$ in x and $0.5m$ in z, nevertheless, the results only are presented in simulation. Also, in [8] are obtained the following parameters: T_s =4s, MS= 14^o and FS=5^o, with $M = 0.791kg$, $m = 0.036kg$ and $l = 70cm$, however, the payload is only transported $0.5m$ in x and $0.5m$ in z, here the payload is moved simultaneously in the two planes. On the other hand, in [12] with $M = 0.710kg$, $m = 47g$ and $l = 62cm$, the payload is moved $1m$ in y with a swing-stabilization time of 4s. In short, even though there exist other works presenting better performances, our work presents an alternative approach to solve the problem of transporting the payload from point to point with swing stabilization.

5 CONCLUSIONS

We obtained a three-dimensional mathematical model via the Euler-Lagrange formalism of an unmanned aerial vehicle transporting a cable-suspended payload with two degrees of the freedom. The equations of motion are expressed in the Hamiltonian formalism. In order to simplify the energy-shaping phase of the control strategy, the mathematical model is represented in two different ways. In the first one, the inertia matrix $\mathcal{M}$ is dependent of q and in the second one, the inertia matrix $\mathcal{M}$ is independent of q.

Furthermore, we have presented an IDA-PBC strategy to stabilize the swing of the payload connected by a cable to a quadrotor. The behavior of the proposed control law was quite acceptable when moving a payload from any initial position to a desired position. Two cases were studied to develop two different control laws. The advantage of the control scheme in the second case is that it does not require an extra measurement for the oscillation angle, since it does not depend on it. Furthermore, the control strategy obtained in the second case was successfully implemented and validated in real-time experiments, employing a monocular vision based algorithm for localization. Hence, it is not constrained to an external motion capture system.

Future work includes extending the control law for the tree-dimensional case and and considering a flexible cable. Also, it would be interesting to design controllers for the trajectory tracking of the swing angle.

References

[1] Bernard M, Kondak K, Maza I, Ollero A. Autonomous Transportation and Deployment with Aerial Robots for Search and Rescue Missions. *Journal of Field Robotics* 2011; **28**(6):914-932.

[2] Hoh RH, Heffley RK, Mitchell DG. Development of Handling Qualities Criteria for Rotorcraft with Externally Slung Loads. *NASA* 2006.

[3] Dai S, Lee T, Bernstein DS. Adaptive Control of a Quadrotor UAV Transporting a Cable-Suspended load with Unknown Mass. *Conference on Decision and Control (CDC)* 2014; 15-17.

[4] Pounds P, Bersak D, Dollar A. Stability of small-scale UAV helicopters and quadrotors with added payload mass under PID control. *Auton Robot* 2012; **33**:129-142.

[5] Nicotra MM, Garone E, Naldi R, Marconi L. Nested Saturation Control of an UAV Carrying a Suspended Load. *American Control Conference (ACC)* 2014; 3585-3790.

[6] Beloti IH, Santos A, Sarcinelli M. Modelling and Control of a PVTOL Quadrotor Carrying a Suspended Load. *International Conference on Unmanned Aircraft Systems (ICUAS)* 2015; 444-450.

[7] Bernard M, Kondak K. Generic Slung Load Transportation System Using Small Size Helicopters. *IEEE International Conference on Robotics and Automation (ICRA)* 2009; 3258-3264.

[8] Goodarzi A, Lee D, Lee T. Geometric control of a quadrotor UAV transporting a payload connected via flexible cable. *International Journal of Control, Automation and Systems* 2015; **13**(6):1486-1498.

[9] Wu G, Sreenath K. Geometric Control of Multiple Quadrotors Transporting a Rigid-body Load. *IEEE Conference on Decision and Control (CDC)* 2014; 6142-6148.

[10] Sadr S, Moosavian A, Zarafshan P. Dynamics Modeling and Control of a Quadrotor with Swing Load. *Journal of Robotics* 2014.

[11] Palunko I, Fierro R, Cruz P. Trajectory Generation for Swing-Free Maneuvers of a Quadrotor with Suspended Payload: A Dynamic Programming Approach. *IEEE International Conference on Robotics and Automation (ICRA)* 2012; 2691-2697.

[12] Palunko I, Cruz P, Fierro R. Agile load transportation. *IEEE Robotics and Automation Magazine* 2012; **19**(3):69-79.

[13] Palunko I, Faust A, Cruz P, Tapia L, Fierro R. A Reinforcement Learning Approach Towards Autonomous Suspended Load Manipulation Using Aerial Robots. *IEEE International Conference on Robotics and Automation (ICRA)* 2013; 4896-4901.

[14] Faust A, Palunko I, Cruz P, Fierro R, Tapia L. Aerial Suspended Cargo Delivery through Reinforcement Learning. *Artificial Intelligence Journal Special Issue on AI and Robotics* 2014; ISSN 0004-3702.

[15] Faust A, Palunko I, Cruz P, Fierro R, Tapia L. Learning swing-free trajectories for uavs with a suspended load. *IEEE International Conference on Robotics and Automation (ICRA)* 2013; 48874894.

[16] Faust A, Ruymgaart P, Salman M, Fierro R, Tapia L. Continuous Action Reinforcement Learning for Control-Affine Systems with Unknown Dynamics. *IEEE/CAA Journal of automatica Sinica* 2014; **1**(3):323-336.

[17] Faust A, Malone N, Tapia L. Planning preference-balancing motions with stochastic disturbances. *International Conference on Intelligent Robots and Systems (IROS)* 2014.

[18] Faust A, Malone N, Tapia L. Preference-balancing Motion Planning under Stochastic Disturbances. *IEEE International Conference on Robotics and Automation (ICRA)* 2015; 35563562.

[19] Cruz P, Fierro R. Autonomous Lift of a Cable-suspended Load by an Unmanned Aerial Robot. *IEEE Conference on Control Applications (CCA)* 2014; 802-807.

[20] Cruz P, Oishi M, Fierro R. Lift of a Cable-suspended Load by a Quadrotor: A Hybrid System Approach. *American Control Conference (ACC)* 2015; 1887-1892.

[21] Sreenath K, Lee T, Kumar V. Geometric Control and Differential Flatness of a Quadrotor UAV with a Cable-Suspended Load. *Conference on Decision and Control (CDC)* 2013; 2269-2274.

[22] Sreenath K, Michael N, Kumar V. Trajectory Generation and Control of a Quadrotor with a Cable-Suspended Load A Differentially-Flat Hybrid System. *IEEE International Conference on Robotics and Automation (ICRA)* 2013; 4873-4880.

[23] Acosta JA, Sanchez MI, Ollero A. Robust Control of Unde-ractuated Aerial Manipulators via IDA-PBC. *Conference on Decision and Control (CDC)* 2014; pp. 673-678.

[24] Souza C, Raffo GV, Castelan EB. Passivity Based Control of a Quadrotor. *19th World Congress The International Federation of Automatic Control (IFAC)* 2014; 24-29.

[25] Souza C, Raffo GV, Milhomem RL, Silva LF, Castelan EB, Moreno UF. Passivity Based Control of a Quadrotor. *XIX Congress Automatic Brazilian (CAB)* 2012; 2303-2313.

[26] Yuksel B, Secchi C, Ulthoff HH, Franchi A. Reshaping the physical properties of a quadrotor through ida-pbc and its application to aerial physical interaction. *IEEE International Conference on Robotics and Automation (ICRA)* 2014.

[27] Guerrero ME, Mercado DA, Lozano R, García CD. IDA-PBC Methodology for a Quadrotor UAV Transporting a Cable-Suspended Payload. *IEEE International Conference on Unmanned Aircraft Systems (ICUAS)* 2015; 471-476.

[28] Guerrero ME, Mercado DA, Lozano R, García CD. Passivity Based Control for a Quadrotor UAV Transporting a Cable-Suspended Payload with Minimum Swing. *Conference on Decision and Control (CDC)* 2015.

[29] Castillo P, Lozano R, Dzul A. Stabilization of a Mini Rotorcraft with Four Rotors. *IEEE Control Systems Magazine* 2005; 45-55.

[30] Ortega R, Spong MW, Gomez F, Blankenstein G. Stabilization of a Class of Underactuated Mechanical Systems Via Interconnection and Damping Assignment. *IEEE Transactions on Automatic Control (TAC)* 2002; **47**(9):1218-1233.

[31] Ortega R, Van der Schaft A, Maschke B, Escobar G. Interconnection and damping assignment passivity-based control of port-controlled hamiltonian systems. *Automatica* 2002; **38**(4):585-596.

[32] Gómez F. and Van der Schaft A. Physical Damping in IDA-PBC Controlled Underactuated Mechanical Systems. *European journal of Control* 2004; **10**(4):451-468.

[33] Klein G, Murray D. Parallel Tracking and Mapping for Small AR Workspaces. *Proc. IEEE Intl. Symposium on Mixed and Augmented Reality (ISMAR)* 2007.

[34] Weiss S, Scaramuzza D, Siegwart R. Monocular-SLAM-Based navigation for autonomous micro helicopters in GPS-denied environments. *Journal of Field Robotics* 2011; **28**(6):854-874.

[35] Engel J, Sturm J, Cremers D. Camera-Based Navigation of a Low-cost Quadrocopter. *Proc. IEEE Intl. Conf. on Intelligent Robot Systems (IROS)* 2002.

[36] Engel J, Sturm J, Cremers D. Scale-Aware Navigation of a Low-Cost Quadrocopter with a Monocular Camera. *Robotics and Autonomous Systems* 2014; **62**(11):1646-1656.

RMS (^{o})	T_s (s)	MS (^{o})	FS (^{o})
5.7438	6.1	19	3
5.3347	5.4	16	4
5.5324	5.9	17	3
5.4143	5.6	17	3
6.0024	6.9	19	3

Table 1
Summary of trials performance for the longitudinal maneuvers.

RMS (^{o})	T_s (s)	MS (^{o})	FS (^{o})
6.3124	5.2	23	6
6.1248	5	21	6
6.5432	5.8	26	6
6.0284	5	20	5
6.6143	6	28	7

Table 2
Summary of trials performance for the transverse maneuvers.

A Appendix

Considering (3), the model (9) through (11) can also be expressed as

$$(M+m)\ddot{\xi}_p - Ml\ddot{\mathbf{r}} + (M+m)ge_3 - fRe_3 = 0 \tag{A.1}$$

$$J\ddot{\eta} + C_r(\eta,\dot{\eta})\dot{\eta} = \tau \tag{A.2}$$

$$\mathbf{r} \times (Mgle_3 - flRe_3 + Ml\ddot{\xi}_p - Ml^2\ddot{\mathbf{r}}) = 0 \tag{A.3}$$

using (A.1) and (A.3) we obtain

$$\mathbf{r} \times (Mgle_3 + Ml\ddot{\xi}_p) = 0 \tag{A.4}$$

also, replacing (A.4) in (A.3) and defining $\dot{w} = \mathbf{r} \times \ddot{\mathbf{r}}$

$$Ml\dot{w} = -fR\mathbf{r} \times e_3 \tag{A.5}$$

let us consider the following equations

$$\begin{aligned}
&\tfrac{d}{dt}(\mathbf{r}\cdot\dot{\mathbf{r}}) = 0 \\
&\mathbf{r}\times(\mathbf{r}\times\ddot{\mathbf{r}}) = \mathbf{r}(\mathbf{r}\cdot\ddot{\mathbf{r}}) - \ddot{\mathbf{r}}(\mathbf{r}\cdot\mathbf{r}) = -(\dot{\mathbf{r}}\cdot\dot{\mathbf{r}})\mathbf{r} - \ddot{\mathbf{r}} \\
&\ddot{\mathbf{r}} = -(\dot{\mathbf{r}}\cdot\dot{\mathbf{r}})\mathbf{r} - \mathbf{r}\times(\mathbf{r}\times\ddot{\mathbf{r}})
\end{aligned}$$

then, by solving $\mathbf{r} \times \ddot{\mathbf{r}}$ from (A.3), equation (A.1) becomes

$$-Ml(\dot{\mathbf{r}}\cdot\dot{\mathbf{r}})\mathbf{r} - \mathbf{r}\times(\mathbf{r}\times(Mge_3 - fRe_3 + M\ddot{\xi}_p)) - (M+m)(\ddot{\xi}_p + ge_3) + fRe_3 = 0$$

Finally, replacing (A.4) in the previous equation gives

$$(M+m)\left(\ddot{\xi}_p + ge_3\right) = \left(\mathbf{r}\cdot fRe_3 - Ml(\dot{\mathbf{r}}\cdot\dot{\mathbf{r}})\right)\mathbf{r}$$